SCIEPublish

Article

Hydrodynamic Performance of a Hybrid Floating Power Dock Combining Multi-Cantilever Type Buoys

Chang Wan [1,2,3], Yuxiang Niu [2], Can Yang [1,2,3,*] and Lars Johanning [1,2,4,*]

[1] College of Shipbuilding Engineering, Harbin Engineering University, Harbin 150001, China; changwan@hrbeu.edu.cn (C.W.)
[2] Yantai Research Institute of Harbin Engineering University, Yantai 264000, China; niuyuxiang@hrbeu.edu.cn (Y.N.)
[3] School of Civil Engineering, University of Queensland, St Lucia, Brisbane 4072, Australia
[4] College of Engineering, Computing and Mathematics, University of Plymouth, Plymouth Campus, Plymouth PL4 8AA, UK

* Corresponding author. E-mail: cyang@hrbeu.edu.cn (C.Y.); lars.johanning@plymouth.ac.uk (L.J.)

Received: 4 November 2024; Accepted: 18 December 2024; Available online: 24 December 2024

ABSTRACT: This paper proposes a novel three-dimensional oscillating pendulum wave energy converter (WEC) that integrates an oscillating float dock station. The device captures wave energy by utilizing both the pitch and roll motions of its primary float and the pendular motion of a buoy. A time-domain analysis method is used to numerically evaluate the hydrodynamic behavior and energy conversion efficiency of the WEC. In ANSYS AQWA, a multi-cantilever WEC model is employed to address the fluid-solid coupling, calculating the device's motion response and capturing the width ratio under various environmental conditions. Additionally, by modifying key geometric parameters including float radius, length, and cantilever angle, the study examines the rotation at the articulation point and the capture width ratio variation for different device configurations. Results indicate that the device achieves a maximum capture width ratio at a float radius of approximately 120 mm under $T = 1.4$ s, and a 130 mm for wave periods of 1.5 s and 1.6 s. The highest average capture width ratio is reached at a power take-off (PTO) damping coefficient of 400 N·s/m. The study further investigates the effect of cantilever angle and float length, aiding in the optimization of these geometric parameters.

Keywords: Wave energy; Hybrid system; Floating dock; Cantilevering type buoy; Potential flow theory; Capture width ratio

1. Introduction

In recent years, small ocean vehicles, particularly autonomous underwater vehicles (AUVs), have emerged as efficient and versatile platforms, significantly contributing to military surveillance and mine detection [1]. Ensuring a reliable power supply for these vehicles is critical, as they must operate for extended durations. While fuel cells [2] can deliver short-term energy, integrating wave energy devices into underwater vehicles offers a convenient and environmentally friendly alternative. Wave energy, recognized as one of the most promising sources of green energy, has garnered increasing attention [3]. The oil crisis of the 1970s marked a pivotal moment in wave energy research [4]. Today, with AUVs becoming increasingly prevalent, systems that enhance their capabilities, extend their operational range, and enable operations in restricted areas have become essential.

One effective strategy for achieving these objectives is the implementation of docking systems [5]. Mao et al. [6] introduced a marine kinetic energy power generation device featuring a two-stage conversion system designed for underwater vehicles. This design minimizes the transfer of intermediate energy, theoretically reducing the device's structural volume while improving the efficiency of the power generation system, thus satisfying the power requirements of unmanned submersibles and similar detection equipment. Additionally, Singh et al. [7] from the Massachusetts Institute of Technology developed an underwater charging platform for AUVs, facilitating remote operation and data transmission between the AUV and the platform. Stokey et al. [8] and Allen et al. [5] explored the docking systems for AUVs and dock stations, enhancing the practicality and reliability of these setups. Hagerman [9] proposed an underwater charging platform for AUVs based on wave energy and the Unitized Regenerative Fuel Cell (URFC). In this design, a buoy harnesses wave energy, activating a hydraulic cylinder to generate high pressure.

https://doi.org/10.70322/mer.2024.10005

Seawater is desalinated using reverse osmosis technology. The purified water serves two purposes: powering the URFC and recharging the AUV's onboard battery. While integrating wave energy devices into underwater submersibles addresses energy supply challenges, maintaining optimal hydrodynamic characteristics and ensuring watertight integrity is essential. Additionally, the low efficiency of wave energy capture often results in longer charging times. To address these challenges, researchers have proposed the concept of underwater docking stations. With ongoing advancements in Power Buoy systems, these devices hold significant potential for offshore power supply and AUV operations. A Power Buoy consists of a vertical column equipped with a conversion system, a heave damping plate and a floating body. The heave damping plate ensures that the column remains as vertical as possible and extends the heave period of the column [10]. When waves act on the heaving floating body, it moves along the column. The relative motion between the floating body and the column facilitates the conversion of wave energy into kinetic energy and subsequently into electrical energy through the conversion system. The generated electrical energy is transmitted via submarine cables to power various systems, supporting signal transmission and charging requirements. Although fixed underwater dock stations exhibit excellent hydrodynamic characteristics, their extensive installation in numerous water areas incurs high layout costs. Consequently, there is a growing trend towards developing mobile wave energy dock stations. These stations harness wave energy to charge their own batteries and AUVs. While charging, the mobile station utilizes its propeller to navigate toward the vehicle, employing a more efficient wireless charging method. This approach reduces the installation costs associated with fixed dock stations and overcomes the limitations of vehicles that cannot carry substantial energy reserves. Moreover, the mobile dock station can continuously recharge its battery, and the wireless charging process enhances efficiency. Furthermore, it can serve as a communication platform for data transmission and other operational functions [11,12].

Computational fluid dynamics (CFD) and potential flow theory are extensively employed to study wave energy converters (WECs) [13]. Potential flow theory, which assumes an ideal fluid, cannot account for real-world phenomena such as viscous friction, turbulence, and eddy shedding, leading to potential inaccuracies [14]. In contrast, CFD methods address these limitations and enhance prediction accuracy [15,16]. However, CFD requires substantial computational resources [17]. Meanwhile, boundary element methods (BEM), derived from potential flow theory, provide faster computations with reasonably accurate predictions [18]. Since its development, AQWA has continuously enhanced, becoming one of the most widely used software tools in the offshore engineering industry [19–21]. Its core functionalities include frequency-domain hydrodynamic analysis, static equilibrium calculation, time-domain simulation, post-processing, and wave load transfer and transformation. AQWA is extensively applied in wave energy research, particularly for devices with relatively simple geometries, enabling rapid computations and efficient parameter optimization across numerous operating conditions. Additionally, AQWA simplifies the handling of boundary conditions, allowing for the easy configuration of various constraints and facilitating coupled multi-physics simulations. With advantages such as high computational accuracy, fast processing speed, user-friendly operation, and excellent visualization capabilities, AQWA stands out as a highly effective tool in offshore engineering applications [22,23].

In this paper, we propose a floating multidimensional oscillating pendulum wave energy converter (OP-WEC) integrated within a flow-type wave energy dock capable of supplying power to marine equipment. Building on traditional oscillating buoy and pendulum wave energy devices, we utilize the potential flow theory of ideal fluids to evaluate the spatial parameter selection of the integrated system under real sea conditions. Our goal is to improve the energy conversion efficiency of the device, while also identifying its operational limits to inform future optimization efforts. Section 2 introduces the model and presents a mathematical model based on potential flow theory. Section 3 verifies the proposed numerical model. Section 4 presents the hydrodynamic performance and energy capture capacity affected by wave conditions and geometric parameters of the device. Finally, Section 5 concludes the paper.

2. Modeling Approach

2.1. Numerical Model

Although buoy-based WECs exhibit excellent energy efficiency and stability, the limitations of single oscillating buoy systems have become apparent as research progresses. These devices often suffer from insufficient energy output and low spatial utilization. To accelerate the development of wave energy systems for larger-scale and commercial use, the concept of integration has emerged as a promising solution. By optimizing the integration and spatial arrangement of WEC, it is possible to enhance energy production and leverage the interactions between floats to improve energy capture efficiency. Traditional buoy-based WECs are frequently integrated into marine structures such as breakwaters and floating platforms. While this integration provides greater stability, it also results in significant wave reflection

effects due to the opaque surfaces of these structures. This reflection can diminish the impact of incident waves and restrict energy capture from waves arriving at the back of the structures [24].

This paper introduces a multi-cantilever oscillating pendulum WEC with a porous structure at the base of the charging platform. This design utilizes three floats to provide buoyancy and restore torque, ensuring high stability while allowing waves to pass through the first float and continue impacting subsequent floats, thereby effectively enhancing energy capture efficiency. The floating multidimensional oscillating pendulum WEC connects multiple horizontal cylindrical floats via hinged joints to a main buoy with a navigation system. The relative motion between the floats and the main buoy drives a hydraulic system that powers a generator, facilitating the conversion of wave energy to kinetic energy and then to electrical energy. The structure of the device, illustrated in Figure 1, includes oscillating floats, a hydraulic cylinder acting as a power take-off (PTO) system, a charging platform, a generator, and a navigation system. During operation, the floats pivot around their hinges in response to wave action, driving the reciprocal motion of connected hydraulic pistons. These pistons operate within bidirectional hydraulic cylinders arranged in parallel, enabling the transmission of high-pressure hydraulic fluid through a network of pipelines. The fluid flow is regulated by an accumulator, which ensures a stable supply to a hydraulic motor, ultimately converting the hydraulic energy into electrical power.

In this study, the motion of the floats primarily occurs in the vertical direction as they rotate around their hinges, while the charging platform experiences six degrees of freedom. A unidirectional hinge links the floats and the charging platform, allowing them to move relative to each other and harnessing this motion to generate electrical energy through the hydraulic system. The device's main buoy features a porous charging platform, offering advantages over traditional buoy structures such as ships and offshore platforms. After waves act on the charging platform, they can continue to affect the next float, potentially enhancing the device's energy capture efficiency. Moreover, the porous design helps mitigate energy loss due to wave reflection. With multiple symmetry axes, the device performs effectively under varying wave directions.

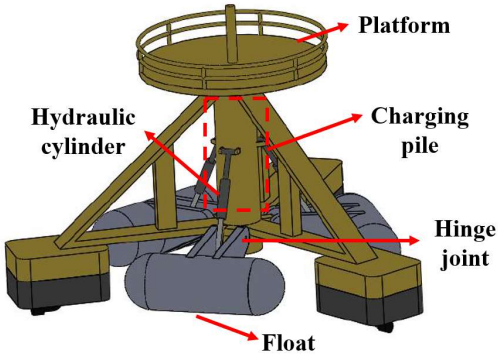

Figure 1. Sketch of the multi-cantilever OP-WEC.

Currently, fluid numerical simulation methods can be broadly categorized into three main types: potential flow linear methods, potential flow nonlinear methods, and viscous methods. Within the linear methods category, there are two sub-types: frequency domain methods and time domain methods. At present, the mainstream software of numerical simulation, including potential flow software AQWA, Hydro STAR, WAMIT and sticky flow software FLUENT, Star-CCM+, have good applications in engineering. To investigate the hydrodynamic characteristics of the floating multidimensional oscillating pendulum wave energy converter (WEC), a numerical model of the device was developed using AQWA software. The simplified numerical model and numerical mesh in AQWA are illustrated in Figure 2. Given the stringent requirements for models in AQWA. It is necessary to simplify the physical model of the floating multidimensional oscillating pendulum WEC, retaining only the key parameters and the hinged constraints between the floats and the charging platform. A scale model with a ratio of 10:1 was employed to reduce both the mesh count and computation time effectively.

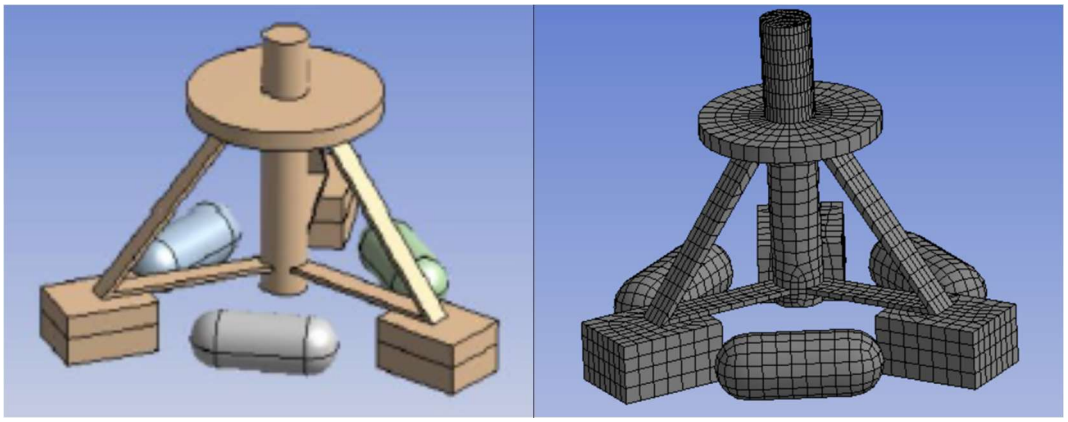

Figure 2. Sketch of the numerical set-up and the computational model established in AQWA.

2.2. Mathematic Methods

Under the action of micro amplitude waves, the floating body has six degrees of freedom of motion: longitudinal, horizontal, vertical, horizontal and bow, assuming that the wave is an ideal fluid without rotation, viscosity and incompressibility, and the incident wave is regular, omitting the second-order term and the infinitesimal term. When the wave acts on the floating body in the flow field, the wave will scatter outward around the floating body. The diffraction wave will form a new wave field after superimposing with the incident wave, and the effect of the superimposed wave field on the floating body is called diffraction. In addition, the floating body will also be affected by radiation. That is, the floating body produces a wave field that radiates outward due to its movement, and the effect of this wave field on the possession is called radiation. Therefore, the velocity potential in the flow field can be represented as the superposition of three components: the incident wave velocity potential, the diffraction potential, and the radiation potential [25]. The expression is as follows:

$$\varphi(x,y,z,t) = \varphi^I + \varphi^D + \varphi^R \tag{1}$$

where Φ^I is the velocity potential of the incident wave, Φ^D is the diffraction potential, and Φ^R is the radiation potential. The velocity potential satisfies the control equation, the free liquid surface condition, the seafloor impenetrability condition, the surface condition, and the infinity condition, and its expression is:

$$\begin{cases} \nabla^2\varphi = 0 \\ \dfrac{\partial^2\varphi}{\partial t^2} + g\dfrac{\partial\varphi}{\partial z} = 0, z = 0 \\ \left.\dfrac{\partial\varphi}{\partial n}\right|_{z=-h} = 0 \\ \dfrac{\partial\varphi}{\partial n} = u n_i \\ \lim\limits_{r\to\infty}\sqrt{r}\left(\dfrac{\partial\varphi}{\partial r} - ik\varphi\right) = 0 \end{cases} \tag{2}$$

Suppose the incident wave is a sinusoidal regular wave propagating in the forward direction along the *x*-axis, and the wave surface equation is:

$$\eta(x,t) = a\cos(kx - \omega t) \tag{3}$$

Taken into the corresponding control equation and boundary conditions, the incidence velocity potential can be obtained:

$$\varphi_i = -\frac{ag}{\omega}\frac{\cosh(z+h)}{\cosh(kh)}e^{ik(x\cos\beta + y\sin\beta)} \tag{4}$$

Among them, the θ is the direction angle of wave propagation, and the diffraction potential and radiation potential are solved by the Green Function Method.

The equations of motion of the float in the time domain are as follows:

$$\{M+\lambda\}\ddot{x}(t)+\int_{-\infty}^{t}\{C(t-\tau)\}\dot{x}(t)d\tau+\{K\}x(t)=F(t) \tag{5}$$

where M is the generalized mass matrix of the floating body, λ is the additional mass matrix, $C(t-\tau)$ is the delay function, K is the floating body's hydrostatic stiffness matrix, and $F(t)$ is the generalized force matrix of the floating body.

Similarly, when a nonlinear power take-off (PTO) system is integrated into the device, time-domain analysis using a scaled model is necessary. This approach effectively reduces the number of meshes and computational time required for the analysis. The interplay between the buoy and the charging pile actuates a hydraulic system, converting mechanical energy into electricity. The charging pile's permeable base enhances efficiency over traditional WECs.

$$\{M+M_{\infty}\}\ddot{x}(t)+\int_{-\infty}^{t}\{C(t-\tau)\}\dot{x}(t)d\tau+\{K\}x(t)+F_{joint}(t)+F_{PTO}(t)=F(t) \tag{6}$$

where M_{∞} is the additional mass matrix when the wave frequency tends to infinity, F_{joint} is the column vector of resistance forces or moments acting as joints in the time domain, and F_{PTO} is the column vector of resistance forces or moments induced by the PTO system in the time domain.

In this device, the joint action is provided by a unidirectional hinge with the constraint equation:

$$A_J x(t)=0,\ A_J^T f_J(t)=F_{joint}(t) \tag{7}$$

where f_J is the local articulated force or moment column vector in the time domain.

In the time domain, the velocity potential of the floating body can be solved by the method of impulse response function, and the velocity potential of the floating body can be expressed as follows:

$$\phi_i(t)=\dot{x}_i(t)\varphi_j+\int_{-\infty}^{t}\dot{x}(t)\chi_j(t-\tau)d\tau \tag{8}$$

where Φ_i is the velocity potential of the floating body in the i^{th} mode, φ_j is the velocity potential induced by the pulse, and χ_j is the velocity potential induced by the pulse after the τ moment.

In the time domain, the floating body is subjected to a radiative force of:

$$F(t)=\iint_s \rho\frac{\partial}{\partial t}\left(\frac{\partial\phi_j(t)}{\partial n}\right)ds=m_{ji}\ddot{x}(t)+\int_{-\infty}^{t}\{C(t-\tau)\}\dot{x}(t)d\tau \tag{9}$$

The total energy of a wave is comprised of two components: kinetic energy and potential energy. The kinetic energy is generated by the movement of the water quality point, the potential energy is generated by the deviation of the water quality point from its equilibrium position, and the total energy expression of the micro amplitude wave is:

$$E=E_k+E_p=\frac{1}{8}\rho gH^2L_w \tag{10}$$

where E_k is the wave kinetic energy, E_p is the wave potential energy, H is the wave height, and L_w is the wave length. Then the wave flow energy of the micro amplitude wave is:

$$P_w=\frac{1}{16}\rho gH^2\frac{\omega}{k}\left(1+\frac{2kd}{\sinh 2kd}\right) \tag{11}$$

where ω is the circular frequency, k is the wave number, d is the water depth, and for floating bodies, the incident wave power P_l within the crest line width is:

$$P_l=D\cdot P_w \tag{12}$$

In the cantilever oscillating float wave energy power generation device, the float harnesses wave energy and transmits it to the generator via the hydraulic system. The coupling effect between the hydraulic system and the oscillating float can be viewed as introducing load damping to the float. The average output power of articulated wave power generation devices is:

$$\overline{P}=\frac{1000\times\overline{T_c}\cdot\overline{n}}{9550} \tag{13}$$

where T_c is the output torque (N·m), which is the damping moment generated by the load damping on the hinge point, and n is the relative speed (r/min), which is the speed at which the float rotates around the hinge point, and the average value can be brought into the formula to obtain the average output power.

The capture width ratio is the ratio of the output power of the device to the wave input power, which is a direct embodiment of the energy capture efficiency of the device, and the calculation formula is:

$$\gamma = \frac{\overline{P}}{P_l} = \frac{\overline{P}}{D \cdot P_w} \tag{14}$$

3. Verification

In order to verify the convergence of the numerical study, three mesh sizes were tested: 0.018 m, 0.027 m, and 0.05 m, corresponding to approximately 18,000, 8000, and 2000 meshes, respectively. Figure 3 shows the heaving displacement for different mesh quantities. The heave displacement results for these mesh sizes were consistent, indicating that the simulation accuracy is largely independent of further mesh refinement within this range. However, testing with a coarser mesh revealed insufficient resolution to capture the boundaries of the floating bodies accurately. To optimize computational efficiency while maintaining simulation accuracy, the 0.05 m mesh size was selected for the numerical analyses. Details of the mesh convergence test and relevant results have been included in the revised manuscript for clarity.

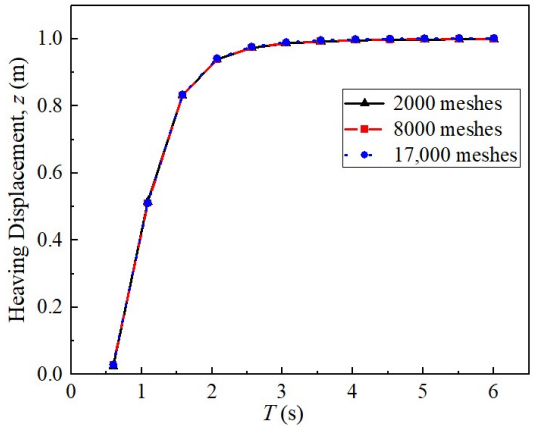

Figure 3. Convergence study for different mesh quantities.

Further, this study verifies the single-body cantilever float model. A horizontally oriented cylindrical float is used, which, with optimized geometric parameters, experiences greater wave forces than traditional vertically oriented floats, resulting in superior power output performance. To validate the numerical model developed, the results are compared against relevant experimental findings on horizontally oriented cylindrical floats conducted by Cai et al. [26]. In the experiment, a horizontally placed cylindrical float was hinged to a movable support, allowing rotation around the hinge point. The influence of varying float mass on device output torque and power output was investigated by adjusting the float mass. For model validation, a replica of the float with matching boundary conditions was created in ANSYS AQWA. Simulations were then conducted with varying float masses to generate output torque and power results for each configuration.

Figure 4 presents a comparison between the numerical simulations and experimental results. The figure shows that the maximum torque and power outputs generated in AQWA are closely aligned with experimental data. The observed discrepancies are likely due to hinge damping and fluid viscosity in the experimental setup, which led to slight energy dissipation, causing experimental values to be marginally lower than the simulated results. Overall, AQWA's calculations strongly agree with experimental results, confirming the feasibility of using AQWA for studying the hydrodynamic coupling characteristics of horizontal cylindrical floats.

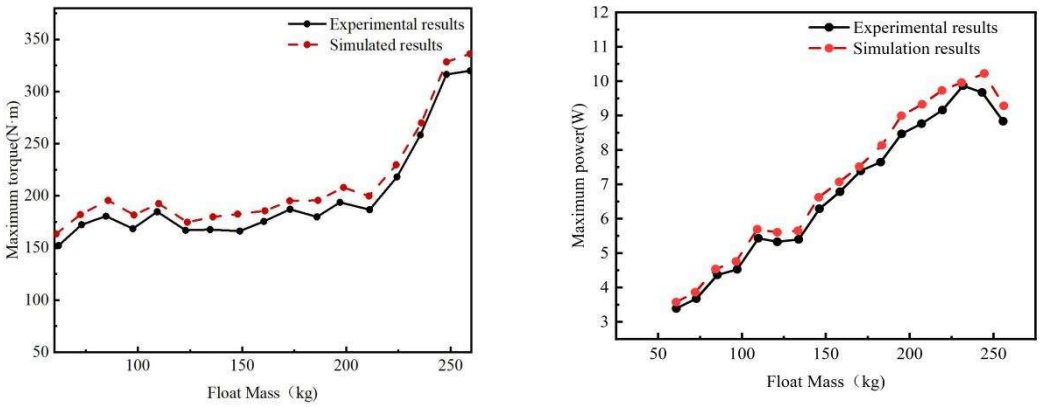

(**a**) (**b**)

Figure 4. Comparison of maximum torque and power between experimental and numerical results. (**a**) Maximum torque; (**b**) Maximum power.

Additionally, to verify the applicability of AQWA in modeling multi-float hinged system, Newman's 1994 dual-float hinged model [27] was employed to assess the accuracy of multi-float model. Two barges, each 40 m in length, 10 m in width, and 5 m in draft, were connected by a unidirectional hinge to analyze the motion response of the hinge point under varying wave frequencies. AQWA was configured with identical model parameters and boundary conditions, including a unidirectional hinge constraint between the barges, and was used to calculate hinge point vertical displacement and vertical force variation across different wave periods. Figure 5 demonstrates a strong correlation between the computed results and those reported by and Zheng et al. [28] and Newman et al. [29], affirming that AQWA is accurate for investigating multi-float hinged systems.

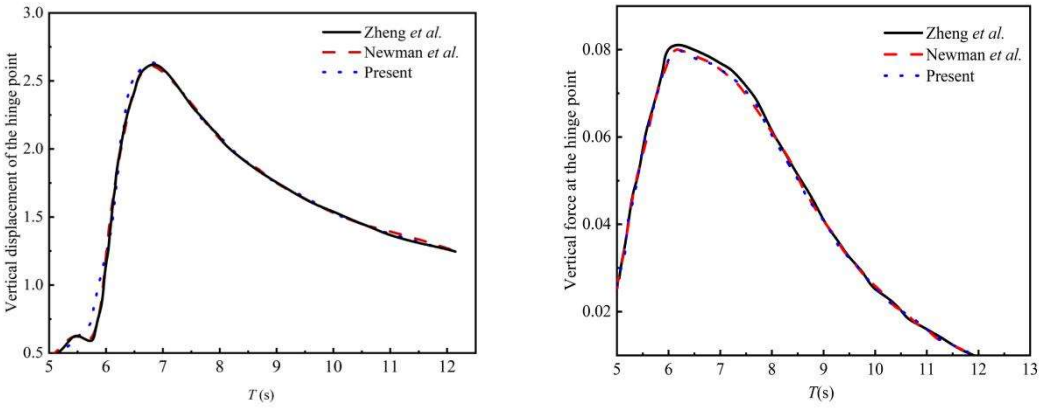

(**a**) (**b**)

Figure 5. Validation of multi-float system. (**a**) Vertical displacement of the articulation point; (**b**) Vertical force at the articulation point [28,29].

4. Results

4.1. Effect of Incident Wave Direction

In the previous research, it is indicated that wave direction significantly impacts the performance of WECs, with the maximum motion response of a single cantilever WEC being approximately three times greater than its minimum response [30]. This study investigates the hydrodynamic and energy capture characteristics of a multi-cantilever oscillating wave energy converter (WEC) under various wave directions. To achieve this, different wave angles are systematically examined. The relative angles and velocities of the floats are examined, providing a basis for determining the optimal deployment orientation of the device. The wave incident directions are categorized in increments of 30 degrees, as illustrated in Figure 6. Float 1 is positioned perpendicular to the 0° incoming wave direction, while Floats 2 and 3 are defined sequentially in a clockwise direction. Due to the device's multiple axes of symmetry, the motion responses are identical for certain incident angles; specifically, the responses are theoretically equivalent at 0°, 60°, 120°, 180°, 240°, and 300°; at 30°, 150°, and 270°; and at 90°, 210°, and 330°. To minimize redundancy from symmetric

wave directions, motion data will be analyzed for wave angles of 30°, 60°, and 90° only. The float dimensions are as follows: radius of 0.12 m, length of 0.36 m, and a draft of 0.12 m. Considering the relatively low wave heights and short periods characteristic of Chinese coastal waters, the selected wave conditions are a height of 0.2 m and a period of 1.6 s.

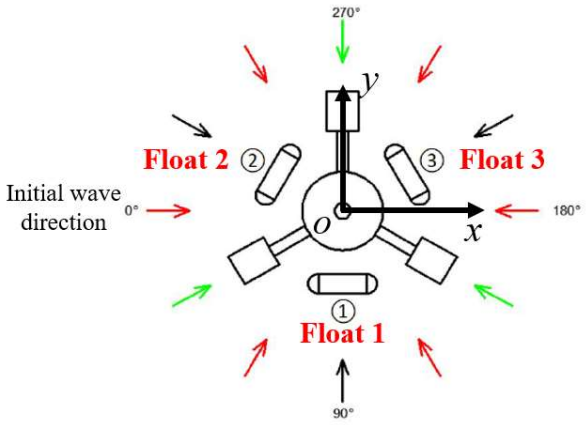

Figure 6. Sketch of wave direction division.

Given that the study involves three floats, using time-history curves to record their motion would result in a large number of curves for each operating condition, making comparison difficult. Therefore, the average value method was adopted to represent the motion of the floats. Specifically, the motion data of each float was integrated and divided by the total time to obtain the time-averaged motion of each float. The average of the time-averaged values for the three floats was then calculated to provide a representative measure of the device's overall motion. Other primary recorded quantities in this study are the data for each float's motion under various wave conditions. These include parameters such as relative turning angle, relative rotation speed and output torque, which were measured throughout the simulation for each operational case.

The time-averaged motion of a single float is obtained by integrating its motion data over the total duration, and the average of the three floats' time-averaged values serves as the assessment standard for the overall device motion. The motion responses of the device under varying wave directions are presented in Figure 7. It is evident that the floats respond differently to waves from various angles. Notably, when waves approach from 60°, Float 1 exhibits the maximum relative angle, reaching approximately 24°. In contrast, Float 3 shows minimal motion response when waves approach from 30°. Considering the device's total energy capture efficiency, the average motion of the three floats is used to characterize the device's overall behavior. The average relative angle at the hinge points for waves from 60° is the largest, approaching 15°. This increased relative angle arises from both the charging station and the floats contributing to the device's motion, as waves from 60° allow for substantial movement in both components. Correspondingly, the average relative velocity of the floats' swing arms is greatest when waves approach from 60°. Compared to single cantilever devices, the multi-cantilever configuration shows a reduction in relative angles and velocities. This decrease is attributed to the waves not directly impacting the floats and the reduced spacing between them, which intensifies mutual interference. Despite the reduction in average relative angle, the incorporation of three hinge points significantly enhances the device's overall power output and energy capture efficiency.Overall, the relative angles at the hinge points exhibit minimal variation across different wave directions. The multi-cantilever device benefits from multiple symmetric wave directions, effectively addressing the issue of unidirectional wave incidence. To optimize average relative angles in future research, all wave incident angles will be set to 60°.

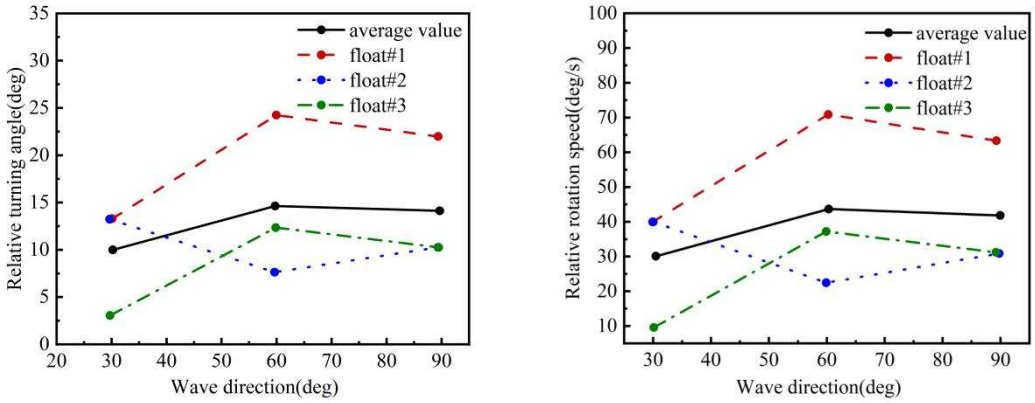

(**a**) (**b**)

Figure 7. Variations of relative angle and relative rotation speed for different wave direction. (**a**) Relative turning angle; (**b**) Relative rotation speed.

4.2. Effect of Wave Height and Period

To explore the suitable wave height conditions for multi-cantilever WECs, this study employs time-domain analysis to examine the variations in hydrodynamic and energy capture characteristics under different wave heights. Based on previous research, wave heights ranging from 0.16 to 0.24 m were selected, maintaining a wave direction of 60° and a wave period of 1.6 s, while other parameters of the device remained constant. The changes in the device's hydrodynamic and energy capture characteristics are illustrated in Figure 8.

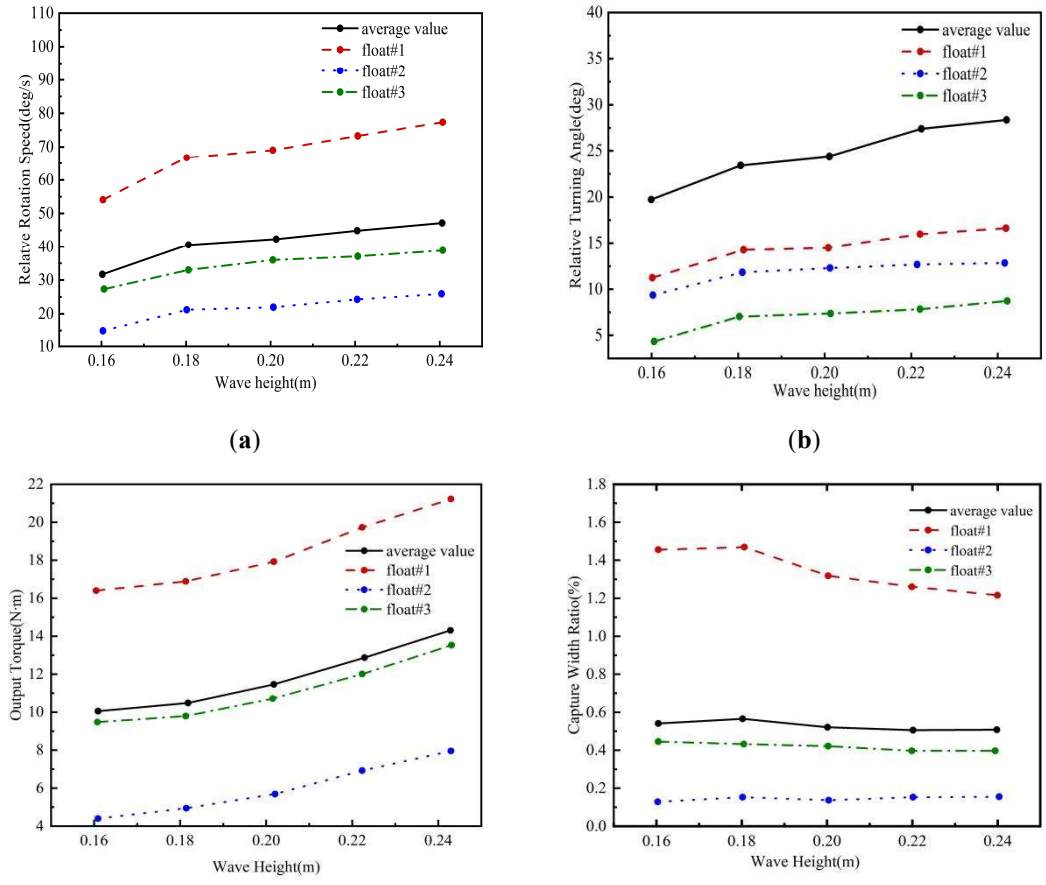

(**a**) (**b**)

(**c**) (**d**)

Figure 8. Variations of relative angle, relative rotation speed, output torque and capture width ratio for different wave height. (**a**) Relative turning angle; (**b**) Relative rotation speed; (**c**) Output torque (**d**) Capture width ratio.

It can be seen in the figure that the relative angles, relative velocities, and output torque of the floats increase with rising wave heights. This trend is primarily attributed to the increased wave energy absorption, which enhances the device's motion response and loading. Although larger wave heights correspond to greater motion responses and power generation, the device's energy capture efficiency varies under different environmental conditions. Consequently, a larger motion response does not guarantee higher energy capture efficiency. As depicted in Figure 8d, the average capture width ratio of the device first increases and then decreases with increasing wave height, reaching a maximum capture width ratio of approximately 0.56 at a wave height of 0.18 m. According to the wave energy calculation formula, the energy of incident waves is proportional to the square of the wave height. Additionally, Figure 8a shows that for wave heights less than or equal to 0.18 m, the relative angle of the device increases rapidly with wave height, which in turn accelerates its ability to capture wave energy. Therefore, for wave heights up to 0.18 m, the capture width ratio exhibits an increasing trend. However, for wave heights exceeding 0.18 m, despite the higher energy of incident waves, the device's ability to capture wave energy increases at a slower rate, resulting in a declining capture width ratio.

The analysis indicates that multi-cantilever WEC exhibits a higher capture width ratio in regions with smaller wave heights. Given the characteristics of China's coastal area, which are characterized by lower wave heights and shorter periods, it can be concluded that these devices are well-suited for deployment in such environments. Moreover, the energy capture capacity of WECs varies under different conditions; therefore, improving wave conditions does not necessarily enhance energy capture efficiency and may increase the risk of damage to the devices in extreme sea states. Therefore, selecting suitable coastal environments and conditions is crucial for the design and installation of wave energy converters (WECs), as this ensures their operational efficiency and longevity.

The wave period is another critical factor influencing the energy capture efficiency of WECs, with varying efficiencies observed across different periods. When the wave period approaches the device's natural frequency, resonance effects occur, significantly enhancing the device's motion response and energy capture efficiency. Given that the mass and geometry of the device affect its natural frequency, and considering the differences between single cantilever and multi-cantilever WECs, it is essential to investigate the hydrodynamic and energy capture characteristics of multi-cantilever devices across different wave periods.

In addition to resonance effects, the energy of the incident waves is another fundamental factor affecting the device's motion response and energy capture efficiency. Wave energy calculation formulas indicate that waves of varying periods have corresponding differences in wavelength. Changes in wavelength, in turn, significantly impact wave energy, ultimately affecting the hydrodynamic and energy capture characteristics of the device. To examine the impact of different wave periods on the device, we set wave periods ranging from 1.3 to 1.7 s, with a wave height of 0.20 m and an incident wave direction of 60°, while keeping other parameters constant. The relative angles, relative velocities, output torque, and capture width ratios of the device are illustrated in Figure 9.

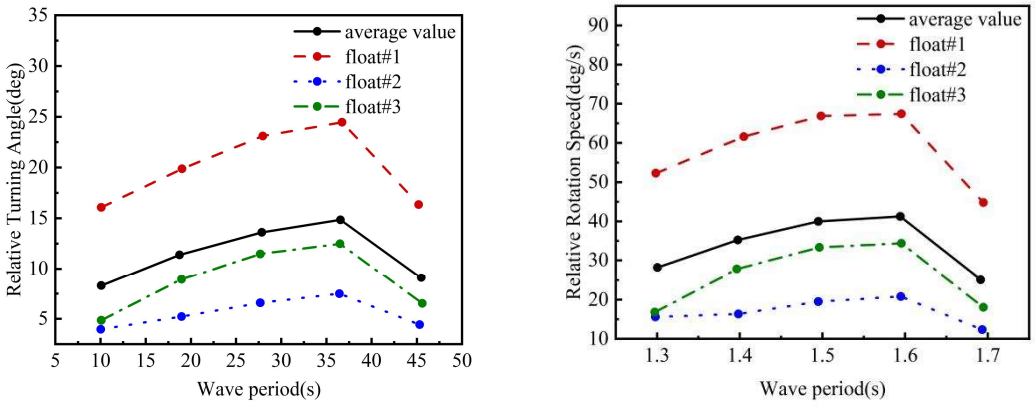

(**a**) (**b**)

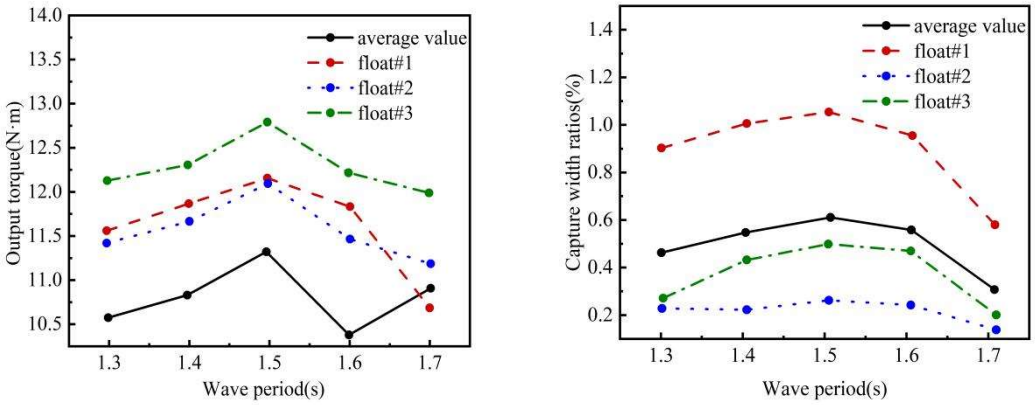

(**c**) (**d**)

Figure 9. Variations of relative angle, relative rotation speed, output torque and capture width ratio for different wave period. (**a**) Relative turning angle; (**b**) Relative rotation speed; (**c**) Output torque (**d**) Capture width ratio.

Figure 9a,b demonstrates that the relative angles and relative velocities at the device's hinge points initially increase and then decrease as the wave period increases. The maximum relative angle and relative velocity occur at T = 1.6 s, while the maximum output torque is achieved at T = 1.5 s. The resonance effect, resulting from the proximity of wave frequency to the device's natural frequency, causes an increase in motion amplitude, suggesting that the natural period of the device is approximately between 1.5 s and 1.6 s.

According to the dispersion relation and wave energy calculation formulas, when wave height and water depth remain constant, the wavelength of the incident waves increases with the wave period, leading to a rise in the energy per unit length of the wave. The WEC's ability to capture wave energy is limited at shorter wave periods. However, as resonance effects emerge, this capability gradually enhances. Because the increase in wave energy is relatively slow, the capture width ratio exhibits an upward trend. As the wave period continues to increase, the wavelength also increases. Still, while the device absorbs more wave energy, much of this energy is allocated to the kinetic and potential energy of the floats and the charging station. This reduced relative motion between the floats and the charging station diminishes the first-stage conversion efficiency of wave energy, leading to a decrease in the capture width ratio. As shown in Figure 9d, the maximum capture width ratio occurs at a wave period of around 1.5 s, reaching approximately 0.58. Compared to single cantilever WEC, the capture width ratio achieved by multi-cantilever configuration through resonance effects is slightly lower. This reduction is primarily due to the denser distribution of floats, which causes significant interference in the surrounding flow field when hinge point motion responses are pronounced. Although the average capture width ratio of the multi-cantilever device is marginally lower than that of the single cantilever configuration, the increased number of floats substantially enhances the overall power generation. Therefore, effectively utilizing the spatial distribution of WEC and the resonance effect can significantly improve their power output and efficiency.

4.3. Effect of Float Radius

The varying waterline areas of floats with different radii result in differing vertical wave excitation forces, leading to distinct motion responses and energy capture capabilities for the device. In a single-cantilever wave energy converter (WEC), comprising only a charging station and a solitary float, the absence of float interactions has a negligible effect on the system's energy capture characteristics. Conversely, in multi-cantilever WEC, the closer arrangement of three floats to the charging station intensifies the interaction between them, significantly affecting the device's energy capture characteristics. Therefore, understanding the influence of float radius on the hydrodynamic and energy capture properties of multi-cantilever devices is essential.

To investigate the effect of float radius on the multi-cantilever device, we set float radii at 100 mm, 110 mm, 120 mm, 130 mm, and 140 mm, respectively, while keeping other geometric parameters constant. The device's natural frequency is partly determined by its mass, which varies with different float radii. Thus, to explore the device's motion and energy capture characteristics near the resonance period, three wave periods are set as T = 1.4 s, 1.5 s, and 1.6 s, with a wave height of 0.2 m and an incident wave direction of 60°. The average values of the three floats' movements were used to evaluate the device's performance in terms of relative angles, relative velocities, output torque, and capture width ratios, as shown in Figure 10.

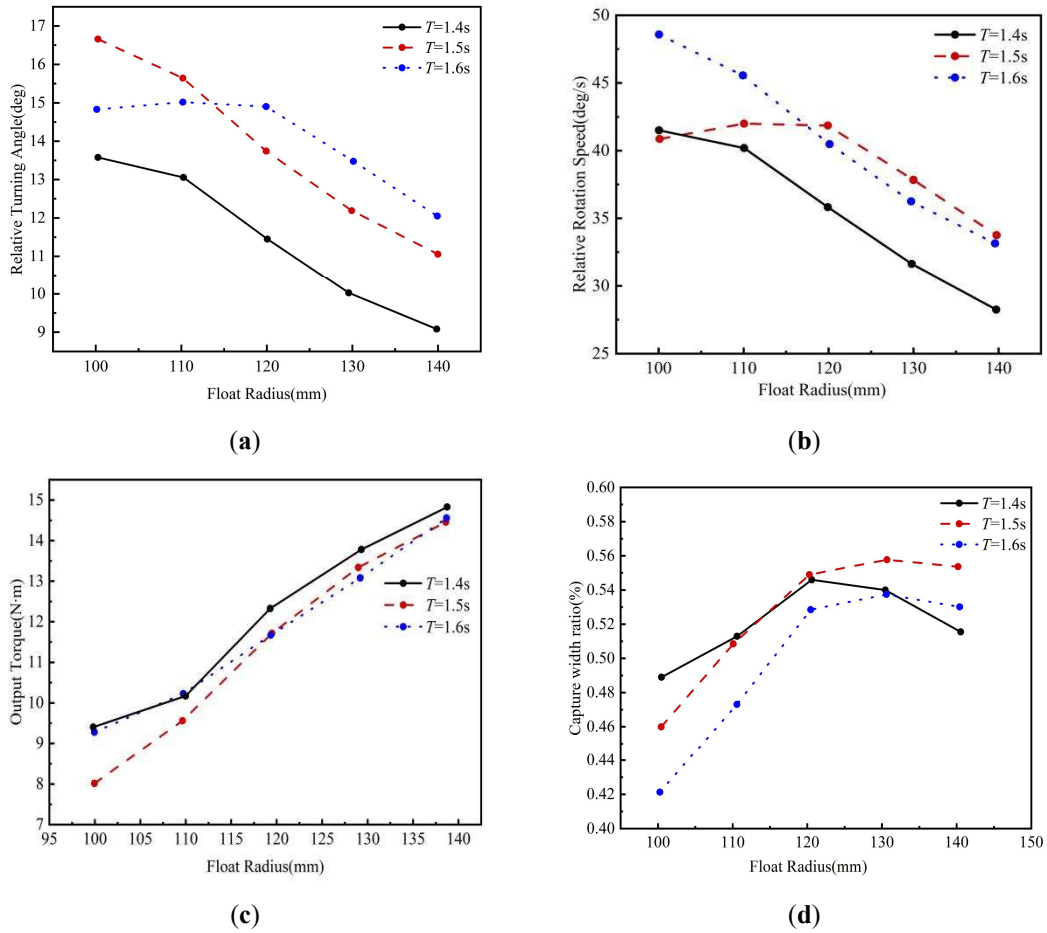

Figure 10. Variations of relative angle, relative rotation speed, output torque and capture width ratio for different float radius under three wave periods. (**a**) Relative turning angle; (**b**) Relative rotation speed; (**c**) Output torque; (**d**) Capture width ratio.

As depicted in Figure 10a,b, the trends of relative angles, relative velocities, output torque, and capture width ratios vary similarly under different wave periods. Notably, at wave periods of 1.4 s and 1.5 s, the device's relative angle and relative velocity decrease as the float radius increases, which is contrary to the motion trends observed in single cantilever devices. However, at a wave period of 1.6 s, the relative angle and relative velocity initially increase with float radius before decreasing. In single cantilever devices, the influence between the float and the charging station is weak, with energy capture primarily dictated by float radius; larger radii result in greater wave excitation forces, thereby increasing the relative angle and relative velocity. In contrast, the multi-cantilever device, which includes three closely arranged floats, experiences heightened interference effects within the flow field. As the float radius increases, although the wave excitation force also increases, the decreased distance between floats leads to increased shielding effects, intensifying negative interference on the flow field and reducing float motion.

In addition, it can be seen that when the float radius is less than or equal to 110 mm, the device exhibits the maximum motion response under wave action at $T = 1.5$ s. Beyond this radius, the motion response increases with the wave period. Figure 10c shows that the output torque of the device increases with float radius, indicating an optimal float radius that maximizes the capture width ratio. According to Figure 10d, at $T = 1.4$ s, the optimal float radius for the maximum capture width ratio is approximately 120 mm. For $T = 1.5$ s and 1.6 s, the maximum capture width ratio occurs at a float radius of 130 mm. Under different wave periods, the capture width ratios for identical float radii vary; specifically, for radii of 100 mm and 110 mm, the maximum capture width ratio occurs at $T = 1.4$ s, while for radii exceeding 110 mm, it peaks at $T = 1.5$ s. Variations in device mass corresponding to different float radii result in differing natural frequencies. Consequently, when analyzing the hydrodynamic characteristics of devices with varying geometries, it is essential to consider the motion responses and energy capture characteristics at other wave periods to determine suitable operational conditions.

4.4. Effect of Float Length

To investigate the influence of float length on multi-cantilever WECs, we varied the float lengths and utilized time-domain analysis to assess the device's motion, subsequently calculating the average capture width ratio of the floats. Float lengths were set at 260 mm, 310 mm, 360 mm, 410 mm, and 460 mm, with adjustments made to float mass to maintain consistent draft. All other parameters remained unchanged, with wave periods set at 1.4 s, 1.5 s, and 1.6 s, a wave height of H = 0.2 m, and an incident wave direction of 60°. Figure 11 illustrates the relative angles, relative velocities, output torque, and capture width ratios of the device.

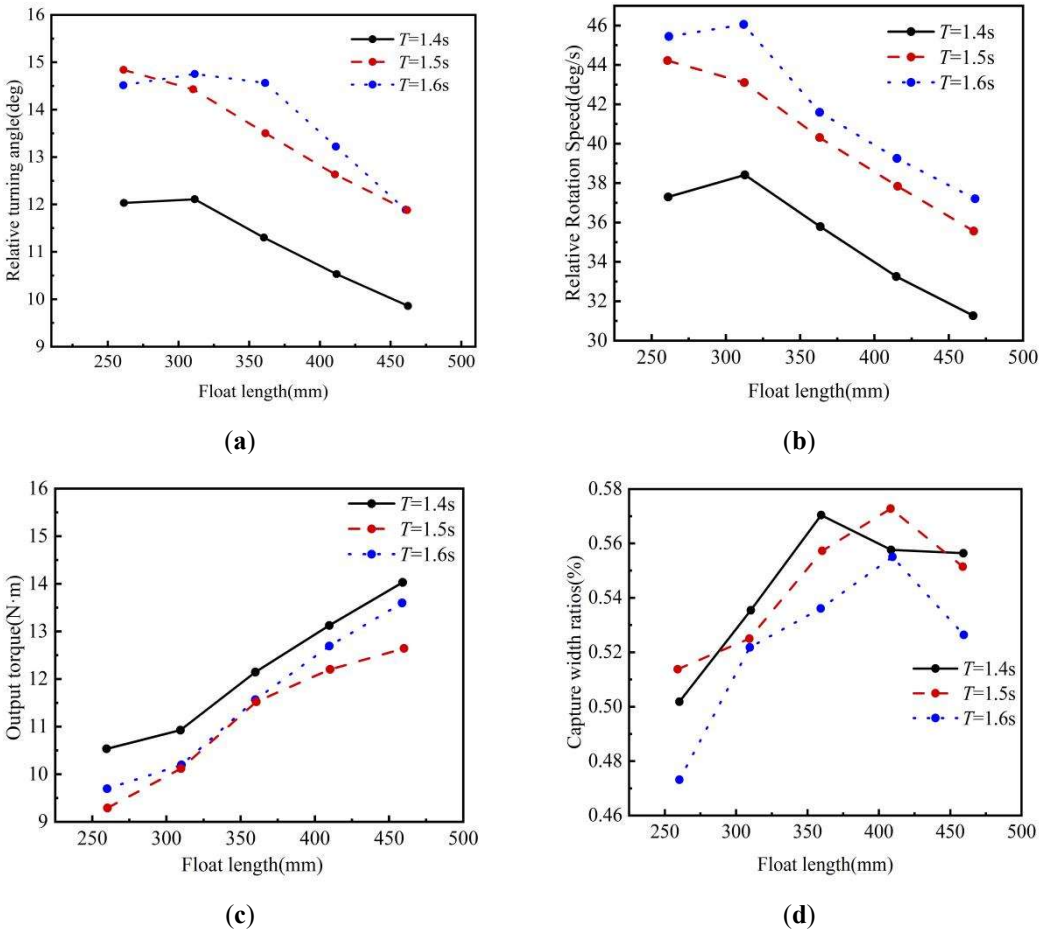

Figure 11. Variations of relative angle, relative rotation speed, output torque and capture width ratio for different float length under three wave periods. (**a**) Relative turning angle; (**b**) Relative rotation speed; (**c**) Output torque; (**d**) Capture width ratio.

As shown in Figure 11, the parameters exhibit similar trends across different periods, with slight variations in magnitude. Figure 11a,b indicates that at T = 1.4 s and 1.6 s, the relative angle and relative velocity initially increase and then decrease as float length increases. In contrast, at T = 1.5 s, these parameters decrease with increasing float length. When the float length is small, the distance between the float and the charging station is larger, resulting in minimal interference in the flow field, with wave forces being the primary influence on float motion. As float length increases, the wave force on the float also increases, enhancing the device's motion response. However, as float lengths increase, while wave forces also rise, the decreased spacing between floats amplifies negative interference effects. This, in turn, reduces the relative angle of motion.

Overall, the motion response of devices with identical float lengths varies under different incident wave periods. Figure 11a,b shows that the device's response is maximized under T = 1.6 s, followed by 1.5 s, with the lowest response occurring at 1.4 s. This variation is attributed to the energy of the incident wave being related to its period; for fixed water depth and wave height, longer wave periods correspond to longer wavelengths and higher energy per unit length. Thus, within a certain range, longer wave periods yield greater motion responses for a given float length. Additionally, changes in float length alter the overall mass of the device, affecting its natural frequency and leading to increased motion responses for specific float lengths under particular wave conditions. As shown in Figure 11c, as float length increases, the output torque also increases. The capture width ratio, calculated according to established formulas,

reaches a maximum at a specific float length. Figure 11d illustrates that the capture width ratio generally increases with float length before decreasing. Under T = 1.4 s, the maximum capture width ratio occurs with a float length of 360 mm, while for T = 1.5 s and 1.6 s, the optimal float length is 410 mm.

4.5. Effect of Initial Cantilever Angle

The cantilever angle of a WEC is defined as the angle between the line connecting the float and the hinge point and the still water surface when the device achieves equilibrium. The relative angle of motion is primarily determined by the float's mass. A larger cantilever angle corresponds to a heavier float, resulting in a greater difference in the relative rotation during positive and negative strokes, which can significantly impact the system, negatively affecting the energy capture capability and potentially shortening the device's lifespan. Conversely, a smaller cantilever angle corresponds to a lighter float, which may not generate sufficient restoring force, thereby diminishing the energy capture efficiency of the device. The hydrodynamic characteristics and energy capture efficiency of multi-cantilever WEC are influenced by the arrangement and coupling distance of the floats. When the cantilever angle is large, the proximity of the floats to the charging station significantly affects their hydrodynamic characteristics, making it challenging to achieve the high energy capture efficiencies seen in single-cantilever devices. Thus, investigating the impact of the cantilever angle on the hydrodynamic performance and energy capture characteristics of multi-cantilever WECs is essential.

To explore this influence, cantilever angles were set at 9.73°, 12.73°, 15.73°, 18.73°, and 21.73°, with all other geometric parameters held constant. Wave periods were set at 1.4 s, 1.5 s, and 1.6 s, a wave height of 0.2 m, and an incident wave direction of 60°. The relative angles, relative velocities, output torque, and capture width ratios of the device are presented in Figure 12. As illustrated in Figure 12a,b, the relative angles and relative velocities of the device under different wave periods first increase and then decrease as the cantilever angle increases. When the cantilever angle is small, the float's mass and draft are also minimal, resulting in a lower restoring force and a smaller amplitude of float movement in response to waves. As the cantilever angle increases, both the float's mass and draft increase, leading to higher wave forces and restoring forces, elevating the relative rotation and velocity. At this stage, the float generates a significant restoring force while maintaining an adequate distance from the other floats and the charging station, resulting in a larger relative angle of rotation. However, further increases in the cantilever angle decrease the distance between the float and the charging station, intensifying negative interference between floats and causing chaotic flow patterns. The superposition of these flow fields results in some energy cancellation, compounded by shading effects between floats, ultimately reducing the relative angle of rotation. When designing a cantilever oscillating float wave energy converter (WEC), selecting an optimal cantilever angle is crucial. This angle must balance enhanced motion response with minimal manufacturing costs and maximum device lifespan. Analysis indicates that when the cantilever angle is less than or equal to 12.73°, the device exhibits maximum motion response under T = 1.5 s; conversely, when the cantilever angle exceeds 12.73°, the motion response increases with the wave period. This variation arises from changes in float mass that alter the system's natural frequency, thereby enhancing motion response when the wave period approaches the device's natural frequency. Conversely, when there is a mismatch between the natural frequency and wave period, the energy associated with the waves increases with the wave period, resulting in increased motion response as the wave period lengthens for a given cantilever angle.

Figure 12c shows that the output torque increases and decreases with increasing cantilever angle. This trend occurs because both very small and very large cantilever angles result in lower relative velocities at the hinge point, thus reducing the output torque. The trends in relative angles, relative velocities, and output torque indicate that the average capture width ratio of the floats also follows a similar pattern, increasing and then decreasing with the cantilever angle. As depicted in Figure 12d, the capture width ratio increases and then decreases with the cantilever angle for various incident wave periods, with a maximum capture width ratio consistently observed at a cantilever angle of 12.73°. When the cantilever angle is less than or equal to 15.73°, the maximum capture width ratio occurs under a 1.4 s wave period; when the cantilever angle exceeds 15.73°, the maximum occurs under T = 1.6 s. Thus, selecting an appropriate cantilever angle is crucial for enhancing the capture width ratio of the device.

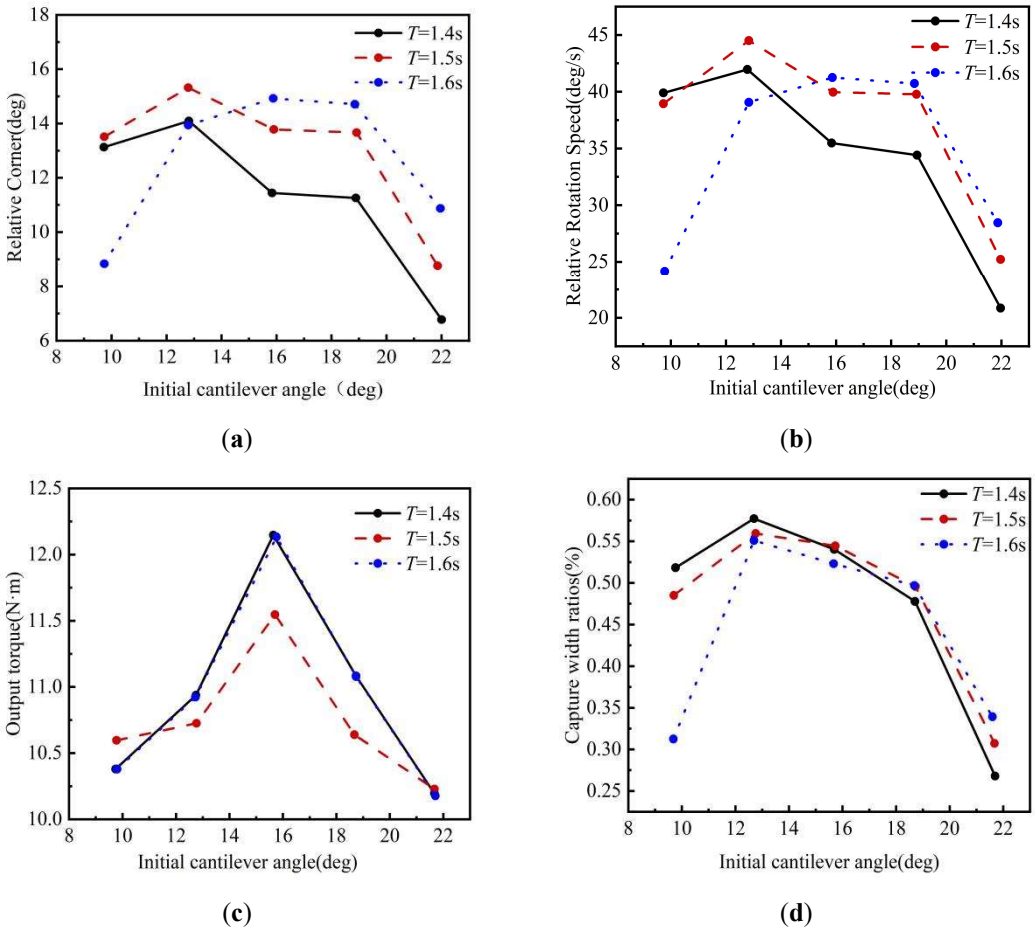

Figure 12. Variations of relative angle, relative rotation speed, output torque and capture width ratio for different cantilever angle under three wave periods. (**a**) Relative turning angle; (**b**) Relative rotation speed; (**c**) Output torque; (**d**) Capture width ratio.

4.6. Effect of Distance between the Cantilever and Charging Pile

In multi-cantilever wave energy converters (WECs), the coupling distance between the float and the charging station plays a critical role in determining the system's hydrodynamic performance and energy capture characteristics. When this distance is small, the shading effect between floats becomes significant, and the negative interference among the floats adversely affects the flow field, leading to energy cancellation and reduced energy capture efficiency. Conversely, a greater distance can hinder the positive influence of the float's radiation potential on other floats. Therefore, investigating the coupling distance between the float and the charging station is vital for understanding the hydrodynamics and energy capture performance of multi-cantilever WEC.

The cantilever distance is defined as the horizontal projection of the line connecting the center of mass of the float to the hinge point. This distance directly impacts the spatial distribution of the floats relative to the charging station, subsequently influencing the device's hydrodynamics and energy capture capabilities. To investigate the impact of cantilever distance on device motion and energy capture characteristics, a series of models were developed with varying cantilever lengths: 275 mm, 315 mm, 355 mm, 395 mm, and 435 mm. All other geometric parameters were held constant. The wave height was set at 0.2 m, with periods of 1.4 s, 1.5 s, and 1.6 s, and the wave direction at 60°. Figure 13 shows various relative angles, velocities, output torque, and capture width ratios of the device.

As depicted in Figure 13a,b, both the device's relative rotation and relative velocity initially increase and then decrease as the cantilever distance increases. This trend is due to the direct impact of cantilever distance on the distribution between the charging station and the floats. When the cantilever distance is short, the proximity of the charging station to the floats leads to significant radiation potential overlap, resulting in considerable interference within the flow field, which reduces the energy available for float motion. Additionally, the close spacing results in substantial shading effects that further impair float movement, decreasing the relative angles and velocities at the hinge point. As the cantilever distance increases, interference among the floats diminishes, and the shading effect between the charging station and the floats is reduced. Consequently, both the relative angles and velocities increase. However, if the

cantilever distance becomes excessively large, the inability to capitalize on the positive effects of radiation potential between the floats leads to a slight decrease in both relative angles and velocities. Moreover, as the distance between floats increases, their mutual interaction decreases, stabilizing the wave forces experienced by each float and causing their motion characteristics to converge. Geometrically, when float movements are similar, a larger radius of motion corresponds to a smaller amplitude of rotation at the hinge point, contributing to the observed decrease in angles and velocities at larger cantilever distances. From the figures, it is evident that with constant wave height, the energy of the incident waves increases with longer wave periods. Consequently, at a fixed cantilever distance, the device's relative rotation and relative velocity increase with longer wave periods.

Additionally, in Figure 13c, the increase in cantilever distance results in a corresponding increase in the lever arm, leading to greater output torque at the hinge point. Figure 13d illustrates that the capture width ratio varies similarly across different incident wave periods, initially increasing and then decreasing with increasing cantilever distance, achieving a maximum capture width ratio when the cantilever distance is 395 mm. The maximum capture width ratio is approximately twice the minimum value. Therefore, selecting an appropriate cantilever distance is essential for significantly enhancing the energy capture efficiency of cantilever-type oscillating float WECs.

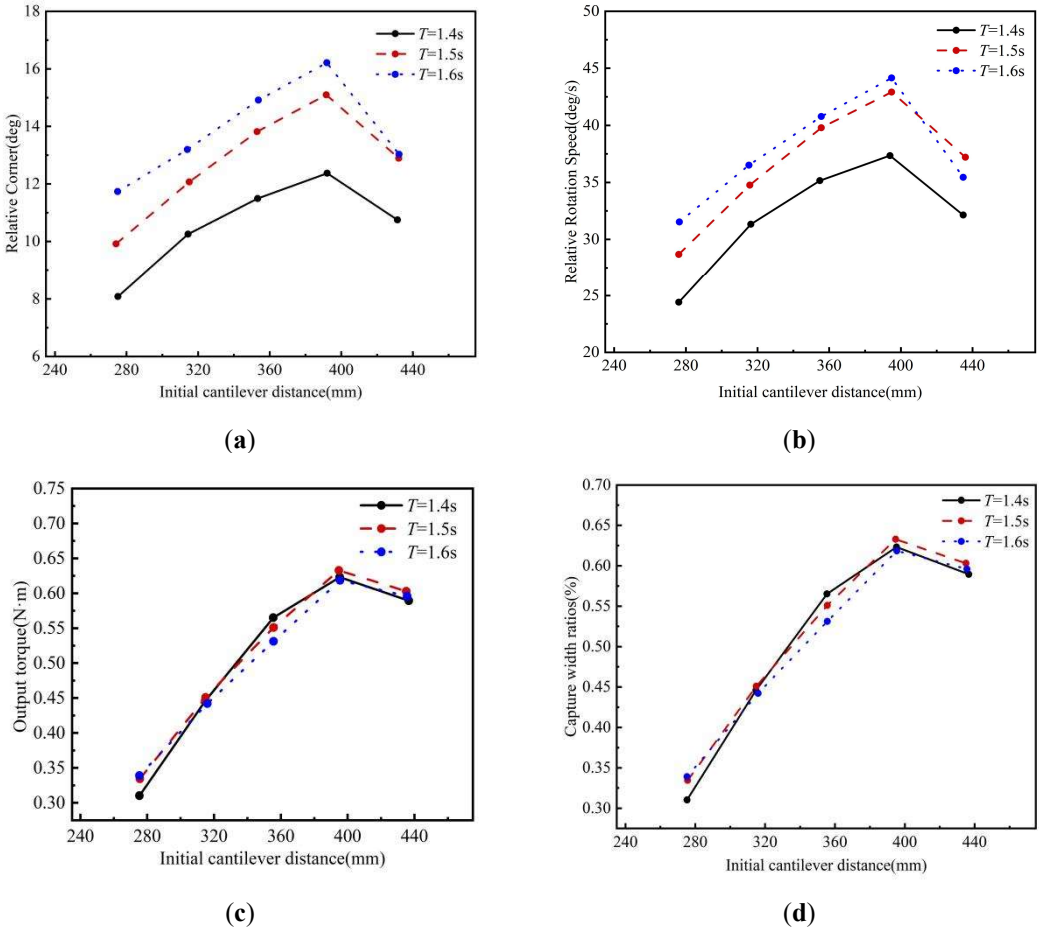

Figure 13. Variations of relative angle, relative rotation speed, output torque and capture width ratio for different distance under three wave periods. (**a**) Relative turning angle; (**b**) Relative rotation speed; (**c**) Output torque; (**d**) Capture width ratio.

4.7. Comparison of the Geometry Parameters

Investigating the energy capture characteristics of multi-cantilever wave energy converters (WECs), we analyzed the impact of device parameters on the capture width ratio, focusing on resonance periods. This analysis led to identifying optimal device configurations for various wave periods, as summarized in Table 1, which presents the parameters before and after adjustments. To optimize the capture width ratio of multi-cantilever wave energy converters (WECs), we developed numerical models with varying parameters and evaluated their performance under specific wave conditions. By comparing the relative rotational speed n (r/min), output torque T_c (N·m), and capture width ratio of the device, the applicable conditions for each setup are outlined. The results for relative speed, output torque, and capture width ratio under different conditions are illustrated in Figure 14.

Table 1. Key parameters of wave and multi-cantilever WEC.

Cases	Wave Period	Wave Angle	Wave Height	Float Radius	Float Length	Cantilever Angle	Cantilever Distance	PTO Damping
1	1.6 s	270°	0.2 m	120 mm	360 mm	15.73°	395 mm	300 N·s/m
2	1.4 s			120 mm	360 mm	12.73°	395 mm	400 N·s/m
3	1.5 s			130 mm	410 mm	12.73°	395 mm	400 N·s/m
4	1.6 s			130 mm	410 mm	12.73°	395 mm	400 N·s/m

As illustrated in the Figure 14, for the device corresponding to Case 2, the capture width ratio reached 0.815 under a wave period of 1.4 s. For the device associated with Case 3, the capture width ratio increased to 0.962 at a wave period of 1.5 s, and for Case 4, it reached 0.925 at a wave period of 1.6 s. Prior to parameter adjustments, the device's capture width ratio was approximately 0.535, indicating a significant improvement in energy capture following these adjustments. Furthermore, the data reveals that following parameter adjustments, the device exhibited increased relative rotational speed and output torque as the incident wave period lengthened. However, the capture width ratio exhibited a trend of first increasing, then decreasing, and finally increasing again as the wave period lengthened. The increase in relative speed and output torque is primarily due to the higher energy associated with longer wave periods, which enhances the device's motion and loading conditions. Despite this, the varying capture capabilities of the device across different wave periods led to a decrease in the capture width ratio at a wave period of 1.6 s, as the rate of increase in incident wave energy outpaced the increases in motion and loading.

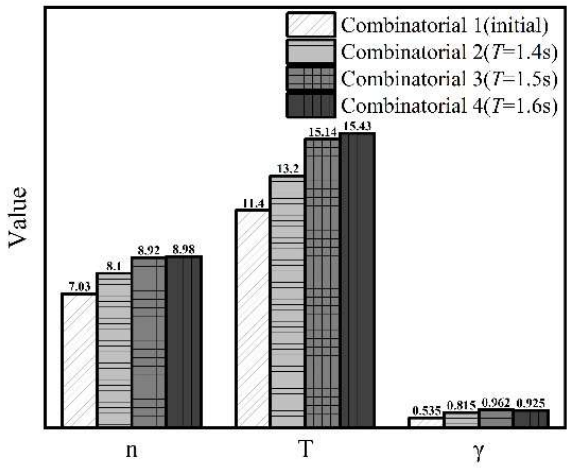

Figure 14. Variations of relative speed, output torque and capture width ratio of multi-cantilever WEC under different wave period and geometric parameters.

Based on previous research, a single-cantilever WEC achieved a capture width ratio of 2 after parameter adjustments, indicating substantial improvement. In contrast, the multi-cantilever WEC, after optimization, achieved an average capture width ratio of approximately 0.962. This disparity is attributed to the denser arrangement of the floats in the multi-cantilever configuration, which results in significant shielding effects between the floats and increased interference with the flow field, thus reducing the capture width ratio. Additionally, greater movement of the device can lead to turbulent flow conditions, which diminish the effective energy, further lowering the capture width ratio.

In this study, although the energy capture efficiency of individual floats in the multi-cantilever WEC is lower than that of the single-cantilever WEC, the overall power generation of the multi-cantilever device is enhanced. Specifically, while the average capture width of each float is smaller than that of the single-cantilever WEC, the multi-cantilever design's multi-axis symmetry allows it to efficiently absorb waves from multiple directions, maintaining a higher overall energy capture efficiency. Additionally, the transparent bottom structure of the charging platform plays a crucial role in improving energy capture. This design allows waves to continue interacting with subsequent floats after passing through the first float, ensuring that the system remains operational and further boosting its energy capture efficiency. Although the average capture width of each float in the multi-cantilever system is smaller than in the single-cantilever WEC, it is important to note that the performance of wave energy devices should not be evaluated solely on capture width. Other factors, such as total power generation, system stability, and operational lifespan, must also be considered. Due to the inclusion of three floats, the multi-cantilever WEC exceeds the single-cantilever WEC in total power output,

which is critical for the device's efficient operation. Moreover, the multi-cantilever system offers enhanced stability. Therefore, while the individual energy capture efficiency of the multi-cantilever WEC may be lower than that of the single-cantilever WEC, its superior total power generation, system stability, and long-term operational feasibility position it as a more promising and capable solution for wave energy conversion.

5. Conclusions

In this study, a novel multidimensional Oscillating Pendulum WEC, which can articulate with a floating docking station, is proposed. This device captures wave energy to charge its onboard battery and is designed to navigate to a vessel requiring charging autonomously. A numerical model of the multi-arm wave energy device was developed and validated against experimental results using simulation software to assess the hinge system. Utilizing time-domain analysis, this study examines the impact of environmental and geometric parameters on the hydrodynamic performance and energy capture characteristics of the device. The research identifies optimal operating conditions and parameter configurations, providing valuable insights for device optimization. The main conclusions are as follows:

(1) The environmental conditions have a less pronounced impact on the motion response and capture width ratio of the multi-arm wave energy device compared to the single-arm device. By selecting the appropriate wave direction and period, the capture width ratio can be moderately improved.
(2) Due to the high spatial utilization of the multi-arm system, where floats and charging piles are densely arranged, increasing the float size, reducing arm spacing, or adjusting arm angles can bring the float surface and charging pile closer, ultimately reducing power generation efficiency. Therefore, selecting an optimal parameter combination is crucial for the multi-arm system.
(3) Optimizing the multi-arm wave energy device yielded substantial enhancements in motion response and energy capture characteristics.Although the capture width ratio per float is slightly reduced compared to a single-arm device, the overall power output is significantly enhanced.

The hybrid floating power dock, featuring a central platform supported by multi-cantilever-type buoys, exhibits several advantages compared to conventional wave energy converter designs. Its structural stability allows it to perform effectively under varying sea states, while the hinged joints and hydraulic cylinders facilitate efficient energy conversion across a broad range of wave frequencies. The modular design simplifies installation and maintenance, and the central platform provides multi-functional capabilities, such as hosting charging infrastructure or supporting maintenance activities. However, the system's structural complexity and the associated costs may pose challenges compared to simpler designs, such as point absorbers or OWCs. Additionally, its larger spatial footprint and sensitivity to wave directionality could limit deployment in areas with constrained space or high marine traffic. Despite these challenges, the hybrid design offers notable scalability and adaptability, making it a promising solution for multi-purpose offshore energy applications. However, this study only examines the device's motion response under regular wave conditions. The response to irregular waves and actual power generation in real sea states requires further investigation. Moreover, as the study's findings are based exclusively on theoretical calculations and simulations, future experimental research is necessary to validate the device's practical performance under realistic sea conditions.

Author Contributions

Conceptualization, L.J. and C.Y.; Methodology, C.Y.; Software, Y.N.; Validation, Y.N.; Formal Analysis, C.W. and C.Y.; Writing–Original Draft Preparation, C.W. and C.Y.; Writing–Review & Editing, L.J.; Supervision, L.J.; Project Administration, L.J. and C.Y.; Funding Acquisition, L.J. and C.Y.

Ethics Statement

Not applicable.

Informed Consent Statement

Not applicable.

Funding

The research was funded National Science Foundation of China (Grant No. 52101306), the National Science Foundation of Shandong Province (Grant No. ZR2021QE121), the British Council (BRI JOINT project), EPSRC ResIn project (EP/R007519/1) and Harbin Engineering University (award to Chang Wan for study abroad at University of Queensland).

Declaration of Competing Interest

The authors declare that they have no known competing financial interests or personal relationships that could have appeared to influence the work reported in this paper.

References

1. Anonymous. *Submerged AUV Charging Station*; NASA Tech Briefs: New York, NY, USA, 2014; Volume 38.
2. Maeda T, Ishiguro S, Yokoyama K, Hirokawa K, Hashimoto AK, Okuda YU, et al. Development of Fuel Cell AUV"URASHIMA. *Mitsubishi Heavy Ind. Tech. Rev.* **2004**, *41*, 344–347.
3. Khaligh A, Onar OC. *Energy Harvesting: Solar, Wind, and Ocean Energy Conversion Systems*; CRC Press Inc.: Boca Raton, FL, USA, 2010.
4. Salter SH. Wave power. *Nature* **1974**, *249*, 720–724.
5. Allen B, Austin T, Forrester N, Goldsborough R, Kukulya A, Packard G, et al. Autonomous Docking Demonstrations with Enhanced REMUS Technology. In Proceedings of the OCEANS 2006, Boston, MA, USA, 18–21 September 2006; pp. 1–6.
6. Mao X, Song B, Zheng K. Design of Generate Electricity Device for Unmanned Underwater Vehicle Based on Ocean Energy. *Meas. Control. Technol.* **2012**, *31*, 127–129.
7. Singh H, Bellingham JG, Hover F, Lemer S, Moran BA, Von der Heydt K, et al. Docking for an Autonomous Ocean Sampling Network. *IEEE J. Ocean. Eng.* **2001**, *26*, 498–514.
8. Stokey R, Allen B, Austin T, Goldsborough R, Forrester N, Purcell M, et al. Enabling Technologies for REMUS Docking: An Integral Component of an Autonomous Ocean-Sampling Network. *IEEE J. Ocean. Eng.* **2001**, *26*, 487–497.
9. Gursel KT. The technological state of the art of wave energy converters. *Adv. Energy Res.* **2019**, *6*, 103–129.
10. Aderinto T, Li H. Review on Power Performance and Efficiency of Wave Energy Converters. *Energies* **2019**, *12*, 4329.
11. Yang C, Wang T, Chen Y. Design and analysis of an omnidirectional and positioning tolerant AUV charging platform. *IET Power Electron.* **2019**, *12*, 2108–2117.
12. Wang T, Zhao Q, Yang C. Visual navigation and docking for a planar type AUV docking and charging system. *Ocean. Eng.* **2021**, *224*, 108744.
13. Wang M, Shang J, Luo Z, Lu Z, Yao G. Theoretical and numerical studies on improving absorption power of multi-body wave energy convert device with nonlinear bistable structure. *Energy* **2023**, *282*, 128904.
14. Anastas G, Santos JA, Fortes CJ, Pinheiro LV. Energy assessment of potential locations for OWC instalation at the Portuguese coast. *Renew. Energy* **2022**, *200*, 37–47.
15. Paduano B, Parrinello L, Niosi F, Dell'Edera O, Sirigu SA, Faedo N, et al. Towards standardised design of wave energy converters: A high-fidelity modelling approach. *Renew. Energy* **2024**, *224*, 120141.
16. Yang I, Tezdogan T, Incecik A. Numerical investigations of a pivoted point absorber wave energy converter integrated with breakwater using CFD. *Ocean. Eng.* **2023**, *274*, 114025.
17. Trivedi K, Koley S, Ray AR. CFD based modeling of OWC device positioned over stepped bottom. In Proceedings of the Energy 2022 7th International Conference on Renewable Energy and Conservation (ICREC 2022), Paris, France, 18–21 November 2022.
18. Sheng W, Tapoglou E, Ma X, Taylor CJ, Dorrell RM, Parsons DR, et al. Hydrodynamic studies of floating structures: Comparison of wave-structure interaction modelling. *Ocean. Eng.* **2022**, *249*, 110878.
19. Ding Q, Li C, Yu N, Hao W, Ji J. Numerical and experimental investigation into the dynamic response of a floating wind turbine spar array platform. *J. Mech. Sci. Technol.* **2018**, *32*, 1106–1116.
20. Hu J, Zhu L, Liu S. Analysis and Optimization on the Flow Ability of Wave Buoy Based on AQWA. In Proceedings of the 2018 5th International Conference on Coastal and Ocean Engineering (ICCOE 2018), Shanghai, China, 27–29 April 2018.
21. Wang YH, Wang JT, Zhang ML, Wu LF, Zhang T. Optimal Design of the Floating Body of the Device of Interception and Diversion for Oil Pollution Based on AQWA and MOGA. *3D Res.* **2018**, *9*, 1–14.
22. KIM SS, PARK BS, KANG DH, LEE JH, CHO HK. A Study on Motion of a Flooding and Un-steerable Vessel in Stormy Weather Condition. *J. Fish. Mar. Sci. Educ.* **2017**, *29*, 286–296.
23. Wang LX, Chen Q, Cao C, Gu Z. Research on hydrodynamic characteristics of conical bottom oscillating float based on AQWA. *IOP Conf. Ser. Earth Environ. Sci.* **2019**, *252*, 032028.

24. Yuan Z, Zhang L, Zhou B, Jin P, Zheng X. Analysis of the Hydrodynamic Performance of an Oyster Wave Energy Converter Using Star-CCM+. *J. Mar. Sci. Appl.* **2019**, *18*, 153–159.
25. Saeidtehrani S, Karimirad M. Multipurpose breakwater: Hydrodynamic analysis of flap-type wave energy converter array integrated to a breakwater. *Ocean. Eng.* **2021**, *235*, 109426.
26. Cai B. *Research on Wave Energy Capture Device of Double Floating Oscillating Float*; Taiyuan University of Science and Technology: Taiyuan, China, 2014. (In Chinese)
27. Davey T, Sarmiento J, Ohana J, Thiebaut F, Haquin S, Weber M, et al. Round Robin Testing: Exploring Experimental Uncertainties through a Multifacility Comparison of a Hinged Raft Wave Energy Converter. *J. Mar. Sci. Eng.* **2021**, *9*, 946.
28. Zheng SM, Zhang YH, Zhang YL, Sheng WA. Numerical study on the dynamics of a two-raft wave energy conversion device. *J. Fluids Struct.* **2015**, *58*, 271–290.
29. Newman JN. Wave effects on deformable bodies. *Appl. Ocean. Res.* **1994**, *16*, 47–59.
30. Wan C, Yang C, Niu Y, Hao Z, Johanning L. Hydrodynamic Investigation on the Cantilevering Oscillating Buoy Type WEC Integrated into a Floating Dock. In *Proceedings of the 11th International Conference on Asian and Pacific Coasts. APAC 2023. Lecture Notes in Civil Engineering*; Tajima Y, Aoki Si, Sato S, Eds.; Springer: Singapore, 2024; Volume 394.